Am J Nucl Med Mol Imaging 2015;5(4):348-362
www.ajnmmi.us /ISSN:2160-8407/ajnmmi0008779

Original Article

Measurement of hypoxia-related parameters in three sublines of a rat prostate carcinoma using dynamic ^{18}F-FMISO-PET-CT and quantitative histology

Pamela Mena-Romano[1], Caixia Cheng[2], Christin Glowa[1,3], Peter Peschke[4], Leyun Pan[2], Uwe Haberkorn[2,5], Antonia Dimitrakopoulou-Strauss[2], Christian P Karger[1]

[1]Department of Medical Physics in Radiation Oncology, German Cancer Research Center, Heidelberg, Germany; [2]Clinical Cooperation Unit Nuclear Medicine, German Cancer Research Center, Heidelberg, Germany; [3]Department of Radiation Oncology, University Hospital Heidelberg, Heidelberg, Germany; [4]Clinical Cooperation Unit Molecular Radiooncology, German Cancer Research Center, Heidelberg, Germany; [5]Department of Nuclear Medicine, University Hospital Heidelberg, Heidelberg, Germany

Received April 4, 2015; Accepted May 1, 2015; Epub June 15, 2015; Published July 1, 2015

Abstract: Hypoxia is an important resistance factor in radiotherapy and measuring its spatial distribution in tumors non-invasively is therefore of major importance. This study characterizes the hypoxic conditions of three tumor sublines (AT1, HI and H) of the Dunning R3327 prostate tumor model, which differ in histology, differentiation degree, volume doubling time and androgenic sensitivity, using dynamic Fluoromisonidazole (^{18}F-FMISO)-Positron Emission Tomography/Computed Tomography (PET-CT) and histology. Measurements were performed for two tumor volumes (average 0.8±0.5 cm^3 vs 4.4±2.8 cm^3). Data were analyzed according to tumor subline as well as to the shape of the time activity curves (TACs), based on standardized uptake values (SUVs) and a two-tissue compartment model. Quantitative immunohistochemical studies of the hypoxic fraction, vessel density and vessel size were performed using pimonidazole, Hoechst 33342 and CD31 dyes. No significant FMISO-uptake was found in small tumors, which had a mean SUV of 0.64±0.36, 0.55±0.10 and 0.45±0.08, for AT1, HI and H sublines respectively. In large tumors, the SUVs were 1.33±0.52, 1.12±0.83 and 0.63±0.16 for AT1, HI and H sublines and the corresponding hypoxic fractions obtained with pimonidazole staining were 0.62±0.23, 0.54±0.24 and 0.07±0.10, respectively. The AT1- was the most and H-tumor was the least hypoxic for both methods ($P<0.05$). All measurements were able to discriminate different hypoxic conditions, however despite SUV and kinetic parameters correlated with the three identified TAC shapes, most of the histological results did not. These results demonstrate impact and limitations of static and dynamic PET-CT measurements to assess hypoxia non-invasively.

Keywords: Hypoxia, dynamic FMISO PET-imaging, pimonidazole, CD31, Hoechst 33342, prostate adenocarcinoma Dunning R3327

Introduction

Tumor growth may lead to a decreased blood supply, that reduces availability of oxygen in the tissue. As a consequence hypoxic conditions in the tumor may occur. Hypoxia is known to increase the resistance against radiotherapy and therefore reduces the chance of a successful treatment [1-3]. To overcome hypoxia, the radiation dose in the tumor must be increased while still respecting the tolerance doses of the surrounding normal tissues. As hypoxia may be heterogeneously distributed, its spatial distribution prior to the treatment has to be characterized.

Several methods exist to measure hypoxia directly or indirectly [3]. So far, the "gold standard" uses polarographic electrode needles that allow direct measure of the partial oxygen pressure (pO_2). Nordsmark *et al.* used polarographic needles and demonstrated, that local tumor control and patient survival in head- and neck-tumors, were significantly correlated with the presence of hypoxia [4, 5]. This method, however, is invasive and can only be used in superficial tumors, does not distinguish between necrotic and viable tissue [6] and in some cases even gives values below zero [7]. Molecular imaging techniques have therefore become of increasing interest as they are non-

invasive and allow repeated three-dimensional (3D) measurements of biological processes *in vivo* [8]. Especially, Positron Emission Tomography (PET) may be used to measure hypoxia using highly specific tracers, that bind to hypoxic regions of the tumor together with the possibility of 3D-images. Among these radiotracers, Fluoromisonidazole (1-(2-nitroimidazolyl)-2-hydroxy-3-fluoropropane) (^{18}F-FMISO) has been most widely studied in clinical and preclinical settings [9-15]. FMISO diffuses passively into the tissue and it is firstly reduced by nitroreductases. In absence of oxygen, further reactions take place, leading to more reactive products that bind to the cell [16]. The detection of FMISO in tumors, has been performed with static and dynamic PET measurements. In the static case, the characterization is based on the SUV, while dynamic measurements use a two-tissue compartment model [17]. The latter apply mathematical modeling to determine pharmacokinetic parameters from the time activity curves (TACs) [18] and some of the resulting parameters are expected to reflect hypoxia. Up to now, however, no correlation between these parameters and pO_2 values in tissue has been found [19].

Prostate tumors can be hypoxic [20-22]. However, only very few clinical studies on the impact of hypoxia in human prostate carcinomas by means of PET, are available [23, 24]. Since the PET-methodology for hypoxia measurements is not yet established for clinical use, preclinical studies are required.

In this study, three sublines (AT1, HI and H) of the rat prostate adenocarcinoma Dunning R3327 have been used to compare different methods for the assessment of their hypoxic status. Although previous studies investigated the hypoxic condition of the anaplastic tumor AT using PET [25-27], this is the first comparative study for three Dunning R3327 sublines. The sublines differ in histology, volume doubling time (VDT), androgen sensitivity, and progression status [28, 29], and thus reflect the heterogeneous nature of clinical prostate tumors. This preclinical study with the varying differentiation status of the sublines, therefore might provide a helpful strategy to further validate the PET technique. To characterize the hypoxic status, we performed static as well as dynamic FMISO-PET evaluations with the use of a two-tissue compartment model. In addition, we used pimonidazole, CD31 and Hoechst 33342 immunofluorescence stainings to quantitatively determine the hypoxic fraction (HF), the perfused vessel density and the mean vessel size.

Materials and methods

Tumor model

Fresh tumor fragments of three different sublines (AT1, HI and H) of the Dunning R3327 rat prostate adenocarcinoma [28-30] were subcutaneously implanted in the distal thigh of young adult male Copenhagen rats (weight, 340.5±55.5 g; age, 9-14 weeks). The AT1-subline was the first anaplastic tumor (AT) that spontaneously arose in rats. It is fast-growing with VDT ~4.8 days. The HI-subline is moderately fast-growing (VDT ~9 days), well differentiated and hormone independent. Finally, the H-subline is slow-growing (VDT ~20 days [31]), well differentiated and hormone-sensitive. The tumor fragments were obtained from a frozen stock, that is maintained as a first passage of the original tumor tissue kindly supplied by Dr. J. Isaacs (John Hopkins University, Baltimore, MD). During PET-measurements, animals were kept under anesthesia with a mixture of Sevoflurane (3%) and air (0.5 l/min). All experiments were approved by the governmental review committee on animal care and the animals were kept under standard laboratory conditions at the German Cancer Research Center.

PET-measurements

In total, 30 tumors (10 AT1, 12 HI, 8 H) were measured by dynamic PET after injection of 15-53 MBq of ^{18}F-FMISO into the tail vein. Measurements were performed at two tumor volumes for all tumors, except of 8 HI that were measured only when tumors were large. The average volume of the small tumors was 0.8±0.5 cm^3 (range 0.1-1.6 cm^3) and 4.4±2.8 cm^3 (range 0.7-16.4 cm^3) for the larger ones. Images were recorded over 60 min using a 28-frame protocol (4 frames of 5 sec, 4 frames of 10 sec, 4 frames of 20 sec, 4 frames of 60 sec, 4 frames of 120 sec, 6 frames of 300 sec and 2 frames of 470 sec). Two rats were imaged simultaneously with a PET-CT (Biograph™ mCT, 128 S; Siemens, Erlangen, Germany) operated in 3-dimensional mode and using an axial field of view of 216 mm. A low-dose computed tomography (80 kV, 30 mA) was used to correct the PET measurement for attenuation. Images

of 400×400 pixels (pixel size 1.565 mm, slice thickness 0.6 mm) were obtained from an iterative image reconstruction, based on the ordered subset expectation maximization algorithm (OSEM) with 6 iterations and 12 subsets. Signal intensities were converted to SUV [32] using a dedicated software (PMOD Technologies Ltd., Zürich, Switzerland).

Data analysis

Tracer uptake in the tumor was measured in a volume of interest (VOI), that was drawn around the maximum SUV using a 75% isocontour. For static data analysis, the maximum SUV in the last frame at 60 min was used.

For pharmacokinetic data analysis, a two-tissue compartment model [33] was fitted to the TAC of the mean SUV in the VOI using PMOD in combination with a modified machine-learning algorithm [34-36]. The arterial input function was obtained from the descending aorta using regions of interest (ROIs) of at least 7 consecutive images [37]. While the first compartment is considered as purely diffusive, the signal in the second compartment reflects the amount of tracer metabolized by hypoxic cells (binding compartment). The corresponding rate constants K_1 (ml/(g·min)) and k_2 (1/min) describe the transport between plasma and the first compartment, while k_3 (1/min) and k_4 (1/min) describe the exchange between the first and the second compartments. In case of hypoxia, k_3 is expected to increase [17]. In addition, the global influx $K_i = \frac{K_1 k_3}{k_2 + k_3}$ is considered as an additional and more stable indicator for hypoxia [38]. This parameter corresponds to an effective transport of the tracer from the plasma into the binding compartment.

In the first step, the differences in SUVs and pharmacokinetic parameters were compared between different tumor sublines. In the second step, we additionally classified the tumors of each subline according to the shape of the TAC, which also provides information about tumor perfusion. For this, we defined three types of TAC: (i) “Decrease” (curves with a perfusion-related peak and a subsequent decrease), (ii) “Increase I” (curves with a small peak and a positive slope at later times), and (iii) “Increase II” (barely noticeable initial peak and increasing uptake thereafter).

Histological preparation

Directly after the second PET-measurement, pimonidazole hydrochloride (60 mg/kg, Hypoxyprobe, Inc., Burlington, MA, USA) was injected into the tail vein. One hour after injection, and 30 seconds before sacrificing the animals, Hoechst 33342 dye (15 mg/kg, Merck KGaA, Darmstadt, Germany) was injected in the right ventricle of the heart. Subsequently, tumors were excised, frozen in isopentane and kept at -80°C until sectioning for immunostaining.

Cryostat sections were immersed in a mixture of methanol/acetone and stored at -20°C. Consecutive slices were stained with H&E, pimonidazole and CD31. The procedure for H&E staining was as follows: sections were stained with Hämatoxylin (Hämalaun, Mayer) for 5 minutes, then washed with flowing water during 10 minutes. Afterwards they were immersed for 1 minute in Eosin (0.5% aqueous solution) and rinsed with distilled water to finally being mounted with Fluoromount-G (Southern Biotech, Birmingham, Alabama, USA).

For pimonidazole staining, sections were blocked against unspecific staining (DAKO, Glostrup, Denmark), then incubated at 4°C overnight with the first MAb1 anti-pimonidazole antibody (1:100, HPI, Inc., USA) in a humid container. The secondary detection was performed using goat anti-mouse Alexa488 IgG antibody (1:2000, Invitrogen Molecular Probes, USA). Cell nuclei were stained with DAPI (Invitrogen Molecular Probes, USA) and washed sections were finally mounted with Fluoromount-G.

For microvessel staining, slices were incubated with mouse anti-rat CD31 antibody (1:500, Merck KGaA, Darmstadt, Germany) for 1 hour, after the blocking against unspecific staining with DAKO. The secondary goat anti-mouse Alexa555 antibody (1:3000, Invitrogen Molecular Probes, USA) was applied to slices and incubated for 30 min. After this time period, slices were washed in phosphate buffered saline (PBS) followed by distilled water and finally mounted with Fluoromount-G.

Quantitative histological image analysis

Sections were imaged at 20× magnification using a Zeiss Axio Observer.Z1 microscope in

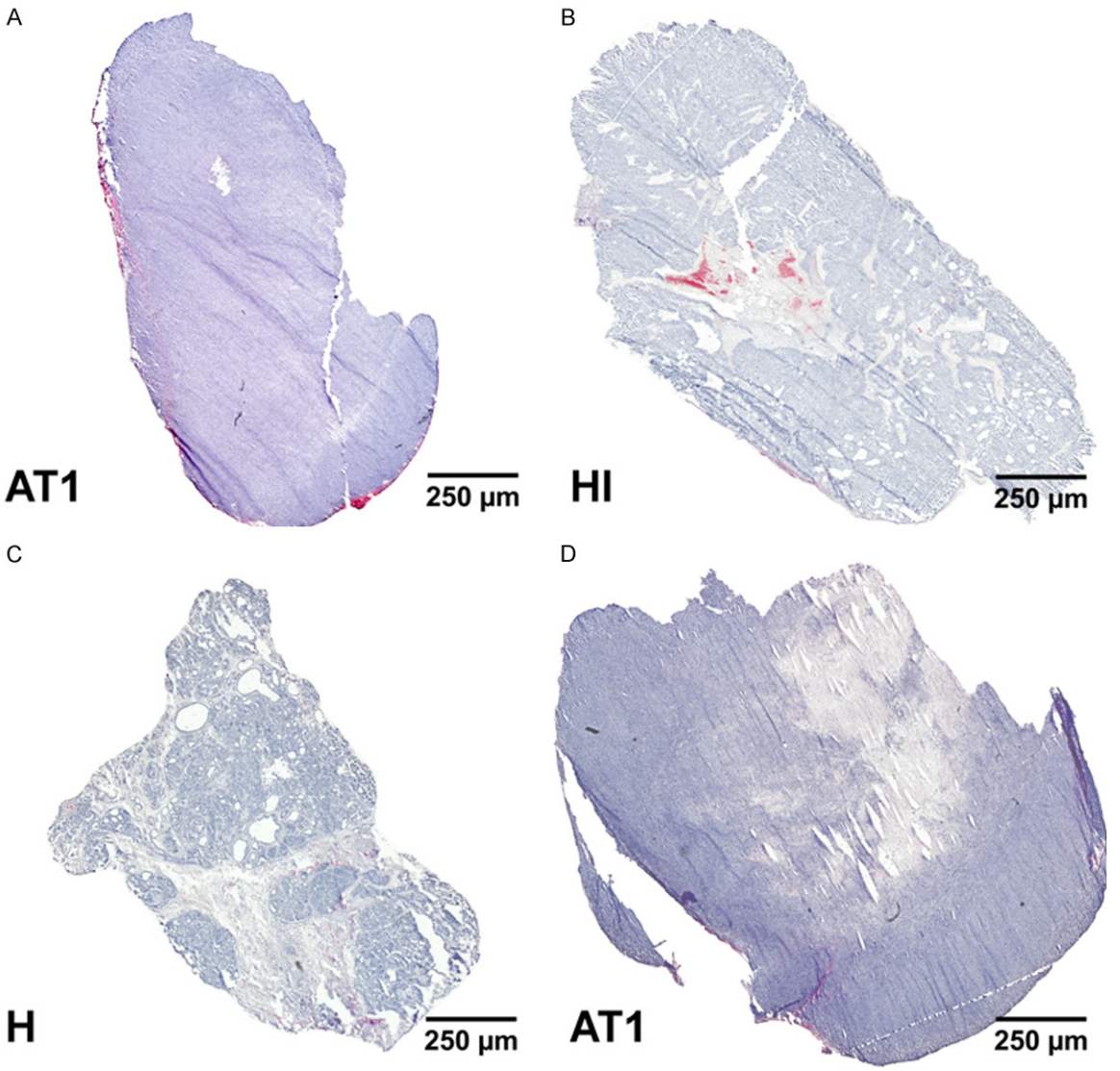

Figure 1. Tumor morphology exhibited in H&E stainings. (A-C) Typical morphology of AT1, HI and H tumors. (D) AT1 with a considerable amount of necrosis (lighter colored).

combination with a Mono Axiocam 506 camera (2752 horizontal pixels ×2208 vertical pixels) and the software Zen pro 2012. Images had a field of view of 604.68×485.15 µm². To obtain representative samples of the tumor, images separated by 1 mm were evaluated along two orthogonal lines across the sections. Tumor borders were excluded from the analysis. Images for CD31 and Hoechst 33342 were consecutively acquired using exposure times of 662 ms with a red and 189 ms with a blue filter, respectively. Pimonidazole and DAPI stainings were acquired with exposure times of 131 ms with a green filter and 87 ms with a blue filter. This procedure was performed for all investigated AT1-tumors. In the case of HI- and H-tumors, some poor quality tissue samples had to be excluded.

Quantitative image analysis of the histological sections was performed with the image processing software Image J (National Institute of Health [39]). For pimonidazole, the background was determined from two contributions: (i) the average signal intensity in controls (n=2 per subline), which did not receive pimonidazole, and (ii) the average signal intensity of the individual tumors, which received pimonidazole, in regions of the section without tissue. This total background was then subtracted from the analyzed images, and the remaining signal was considered as pimonidazole positive. Hypoxic fraction (HF) was measured as the area of posi-

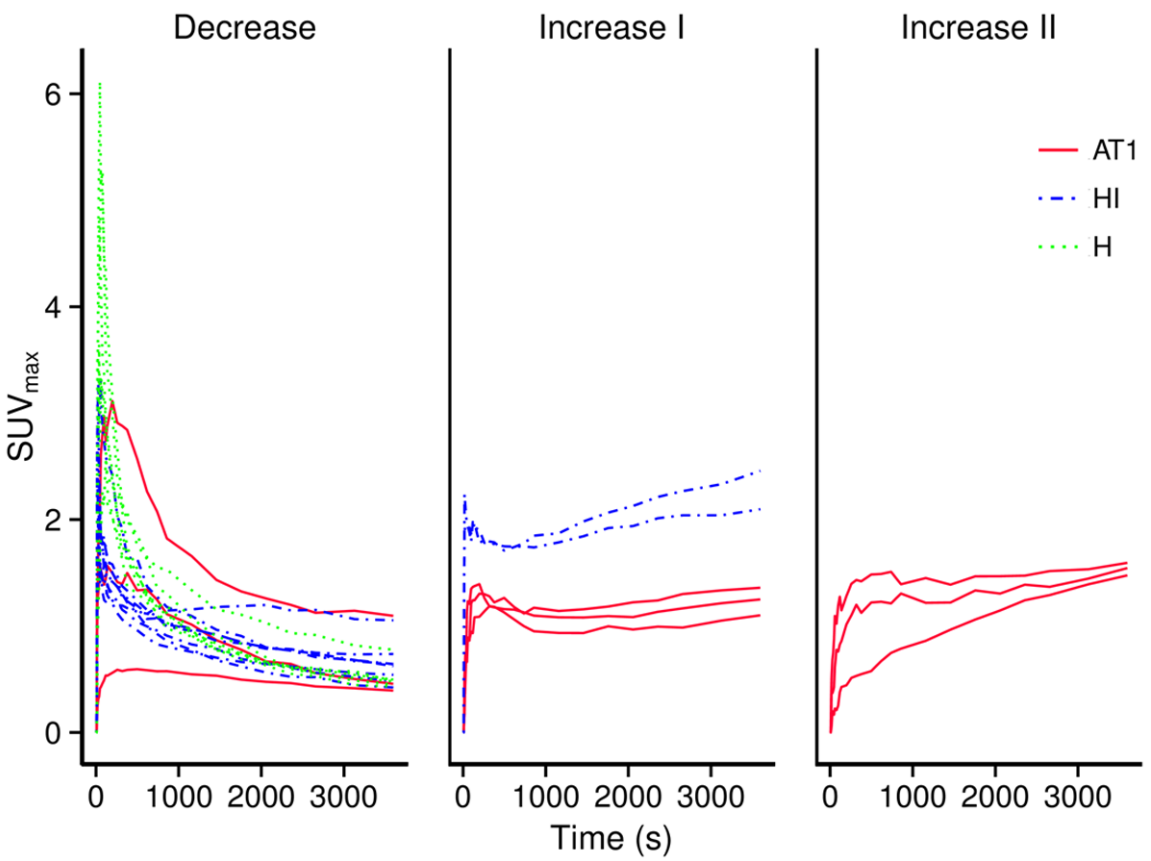

Figure 2. Heterogeneity between and within tumor sublines. Time activity curves (TACs) classified according to their shape. Each curve corresponds to an individual tumor.

tive pimonidazole staining divided by the tissue area of the analyzed image section, excluding the vacuoles.

Vessel density was calculated by the manually counted number of CD31-stained vessels after background subtraction divided by the evaluated tissue area. Vessels were identified when the staining was continuous along a straight (vessel in plane) or circular (vessel across plane) line. Background was estimated as the average signal of CD31 negative areas of the analyzed image and was subtracted from the entire image. To estimate the size of each vessel (in μm^2), an automatic counting was performed using the "analyze particles"-command in ImageJ and setting the minimum particle size to 20 μm^2. Finally, the number of perfused vessels was calculated by manually counting Hoechst 33342-positive vessels.

Statistics

Statistical significance was tested pairwise using the two-sided Mann-Whitney U test for independent samples in the software R [40]. A *P*-value below 0.05 was considered as statistically significant.

Results

The different morphological architecture of the 3 sublines is documented by H&E-stainings. **Figure 1A-C** reveal the typical morphology of the three sublines. For the AT1, some of the tumors were characterized by a high amount of necrosis mainly in the central region (**Figure 1D**).

Figure 2 shows the TACs used as basis for the static and dynamic PET-analysis. Within the TACs, we found a large heterogeneity even within one subline. While the AT1-subline showed all three different kind of TAC shapes, the HI-subline exhibited only the types "Decrease" and "Increase I" and the H-subline depicted only the "Decrease" type.

PET-measurements analyzed by tumor sublines

Two animals (one AT1- and one HI-tumor) of the first measurement series containing tumors of

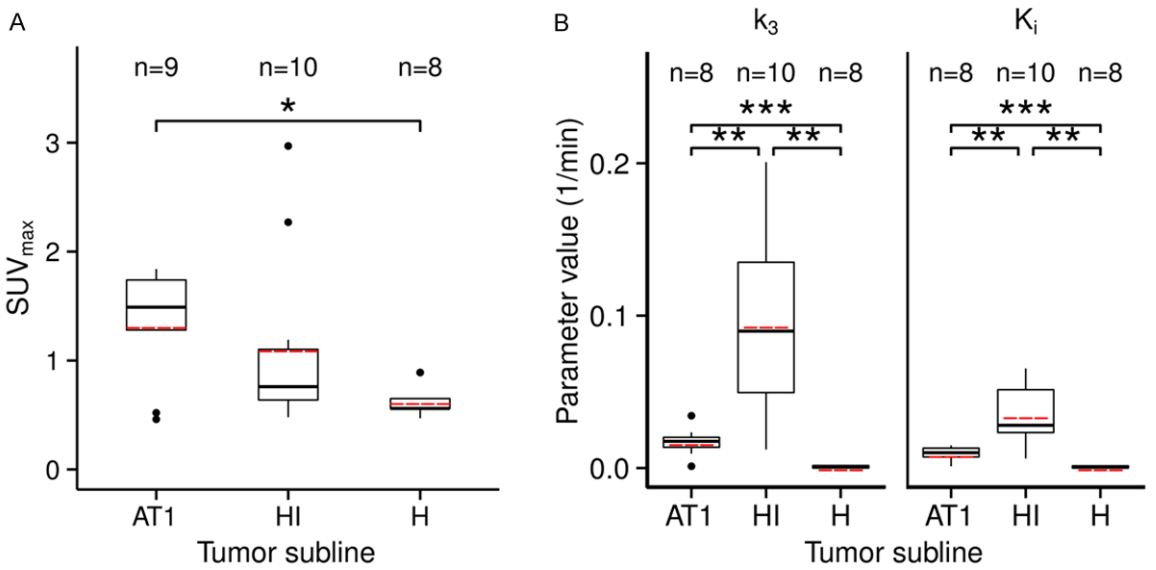

Figure 3. PET hypoxia parameters. (A) Maximum SUV for the three tumor sublines. The two outliers of the AT1 showed significant amount of necrosis, where tracer is not bound. (B) Kinetic parameters (k_3 and K_i) according to the subline. All sublines differ significantly. One AT1 outlier (k_3=0.66 and K_i=0.10) is not shown. Solid line: median, dashed line: mean, box: 25/75 percentile, upper whisker: extends from the upper hinge to the highest value within 1.5×IQR (inter quartile range), lower whisker: extends from the lower hinge to the lowest value within 1.5×IQR, dots: outliers, *P<0.05, **P<0.01, ***P<0.001 and n corresponds to the number of tumors per subline.

small volume were excluded from the evaluation due to problems with the tracer injection. The remaining animals did not show significant uptake in the tumors (mean SUV of 0.64±0.36, 0.55±0.10 and 0.45±0.08 for AT1, HI and H sublines, respectively). Another three animals (one AT1- and two HI-tumors) of the second measurement with tumors of larger volumes were also excluded due to injection problems. The SUVs are shown in **Figure 3A** and the mean SUVs were 1.33±0.52 (AT1), 1.12±0.83 (HI) and 0.63±0.16 (H). The difference between the AT1- and the H-sublines was significant.

The values of the fitted kinetic parameters k_3 and K_i differed significantly between all sublines (**Figure 3B**). However AT1- and H-tumors had smaller and less dispersed values than HI-tumors.

Histological images analyzed by tumor sublines

Figure 4A-C show representative images of pimonidazole and DAPI stainings for each tumor subline. The hypoxic fraction estimated for all sublines ranged from 0 to 0.97 (**Figure 4D**). One AT1-tumor was excluded from the analysis because of technical problems. The AT1-subline was found to be the most hypoxic (mean hypoxic fraction: 0.62±0.23), while the other sublines showed smaller values of 0.54±0.24 (HI) and 0.07±0.10 (H). The difference between all sublines was statistically significant. The H-subline was the most homogeneous in terms of hypoxia (range 0-0.42), while the AT1- and HI-sublines had a very large spread (0-0.97 and 0-0.94, respectively). The hypoxic fraction (HF) was also analyzed along the tumor profile from the periphery to the center, and no differences were found in HI- and H-sublines, however, AT1-images exhibited a nearly significant (P=0.052) higher HF in the center of the tumor in comparison to the periphery (**Figure 4E**).

Figure 5A-C displays representative images of CD31 and Hoechst 33342 stainings for the three tumor sublines. When calculating the percentage of perfused vessels, we found an average fraction of 71% for the AT1, while the HI- and H-tumors were characterized by higher values of 94% and 92%, respectively. The perfused vessel density varied for all sublines. Especially for the AT1-tumor, a range from 0 to 451 vessels/mm^2 was seen, however most of the images contained less than 50 vessels/mm^2. In average, 101±131, 71±67 and 174±69 vessels/mm^2 were recorded for AT1-, HI- and H-tumors, respectively (**Figure 5D**). The relative number of images containing only non-perfused vessels (first bin for AT1 and HI in **Figure**

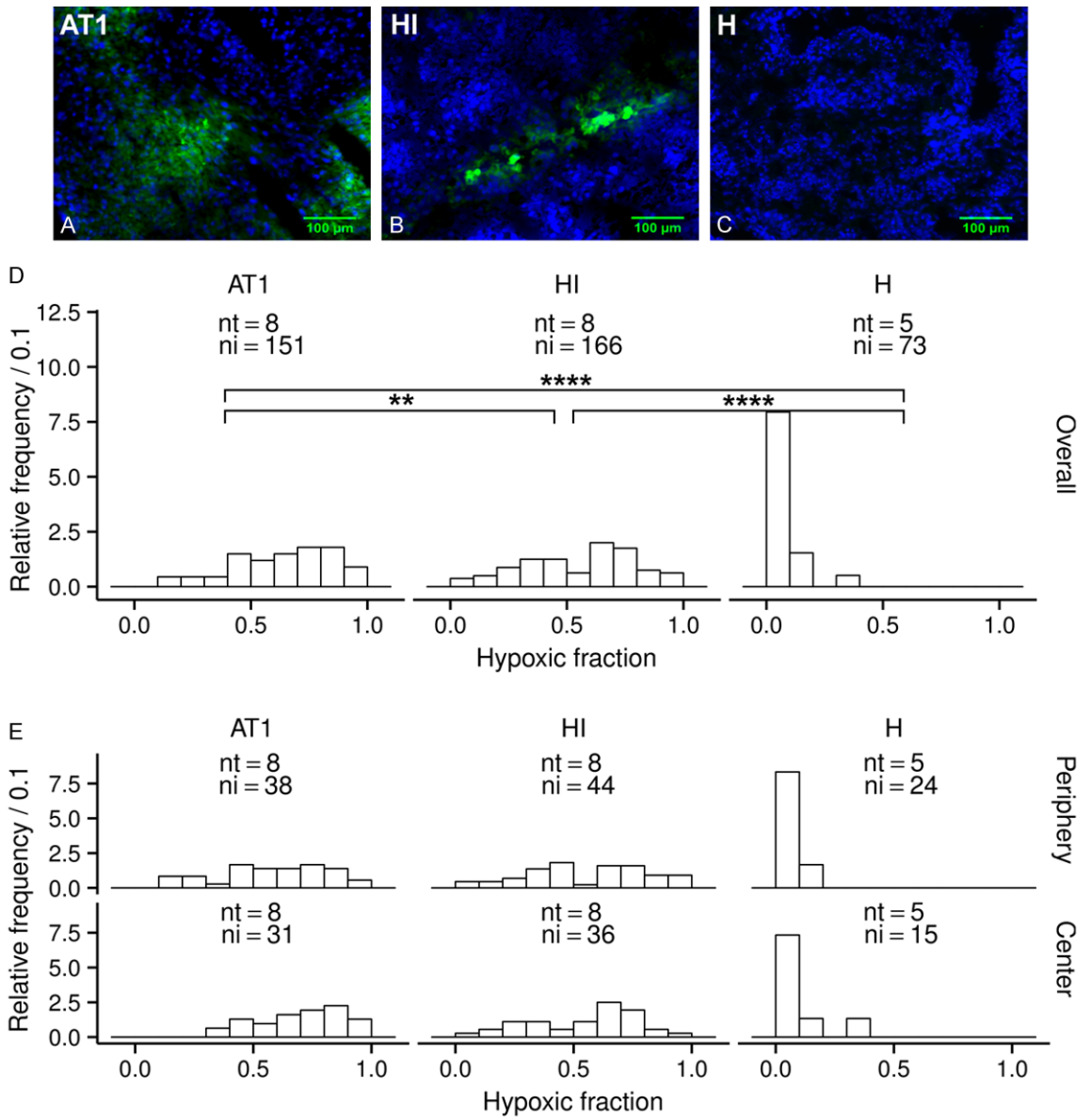

Figure 4. Histological results for pimonidazole staining. (A-C) Representative images with pimonidazole (green) and DAPI (blue) stainings. (D) Hypoxic fraction per image, estimated from pimonidazole staining for the three tumor sublines. (E) Hypoxic fraction per image, according to the image position in the tumor for each subline. nt and ni are the number of analyzed tumors and images, respectively. **P<0.01 and ****P<0.0001.

5D) is shown according to their position within the tumor (**Figure 5E**), with 0 and 1 referring to the periphery and 0.5 to the center of the tumor respectively. Only the AT1-subline revealed an increased number of non-perfused images from the periphery to the center of the tumor (correlation coefficient of 0.93 and -0.77 for the ranges 0 to 0.5 and 0.5 to 1.0, respectively).

H-tumors had a mean vessel size of 140.0±54.2 µm². In contrast AT1- and HI-sublines had smaller vessels with an average of 90.5±59.4 and 109.0±85.4 µm², respectively. HI-tumors were found to be the most heterogeneous subline with a range of 33.14-722.0 µm², while the AT1- and H-sublines ranged from 21.4 to 480.8 and 39.5 to 288.0 µm² respectively (**Figure 5F**).

PET-measurements analyzed by TAC-shapes

Figure 6 shows the analysis of the PET related parameters (SUV, k_3 and K_i) according to the TAC-shape. Compared to the "Decrease" type,

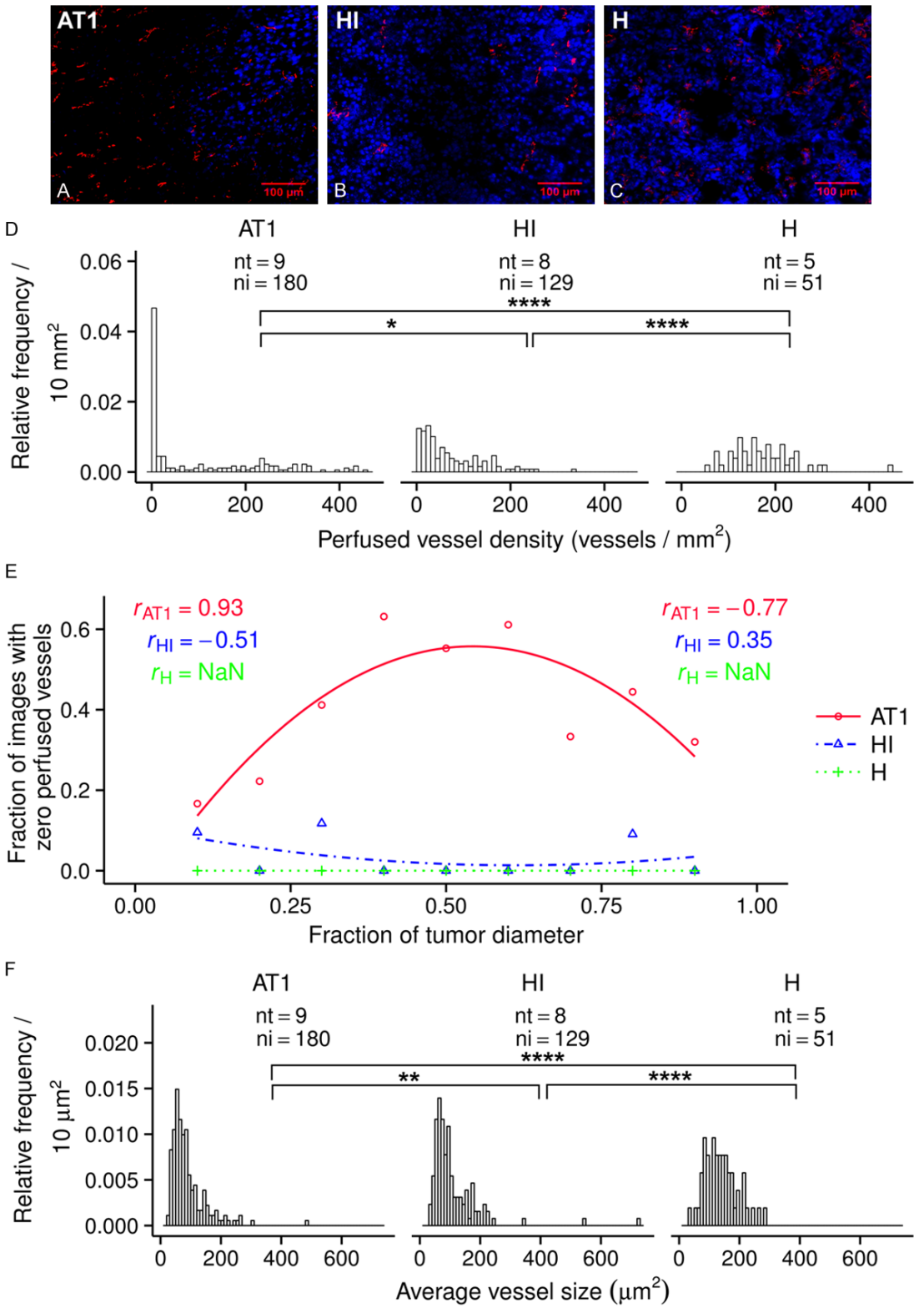

Figure 5. Histological results for CD31 and Hoechst stainings. (A-C) Representative images with CD31 (red) and Hoechst 33342 (blue) stainings. (D) Number of perfused vessels per image for each tumor subline, obtained with CD31 and Hoechst 33342. (E) Relative frequency of images without perfused vessels, organized according to their position in the tumor (0 and 1 refer to the tumor edges and 0.5 to the center) and fitted with a second order polynomial. Correlation coefficients from position 0 to 0.5 and from 0.5 to 1 are shown in the left and right legend, respectively. (F) Average vessel size per image for each subline. (Histograms show normalized frequency/bin size. *P<0.05, **P<0.01, ****P<0.0001 and nt and ni are the number of analyzed tumors and images, respectively).

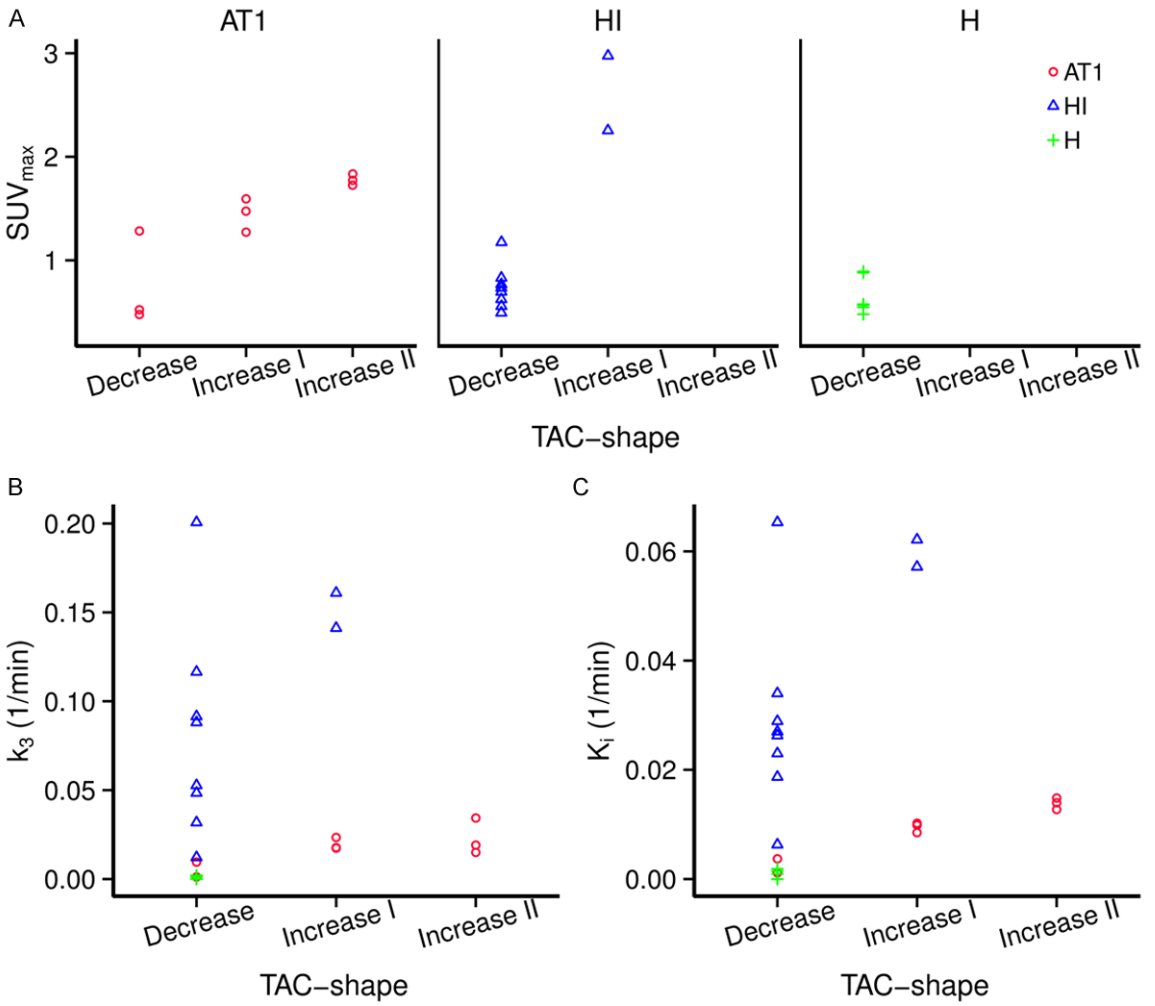

Figure 6. PET parameters separated according to tumor TAC-shape for all sublines. (A) SUV and the kinetic parameters (B) k_3 and (C) K_i.

AT1- and HI-sublines categorized as "Increase I and II" and "Increase I" respectively, exhibited higher SUVs. In the case of AT1, the maximum SUV was found in the "Increase II" type (**Figure 6A**). Regarding the kinetic parameters (**Figure 6B** and **6C**), AT1- and HI-sublines showed the highest average of K_i values in "Increase II" and "Increase I" types, respectively.

Histological images analyzed by TAC-shapes

The histological parameters were also classified according to the TAC shapes (**Figure 7**). No differences in hypoxic fractions between these, were found for the AT1-subline. Its average was 62±21% in the "Decrease" group, 59±23% in the "Increase I" and 64±24% in the "Increase II" group, respectively. In the HI-subline on the other hand, a significant increase of the hypoxic fraction from 48±25% in the "Decrease" group to 66±20% in the "Increase I" group was detected. When comparing the three different sublines, AT1-tumors were characterized by the largest hypoxic fraction in the "Decrease" group (**Figure 7A**).

For AT1-tumors also the number of perfused vessels varied according to TAC shapes with 36±76 vessels/mm² (mean ± SD) in the "Decrease" group, 259±112 in "Increase I" and 84±117 vessels/mm² in the "Increase II" type. In contrast, HI-subline, showed a nearly constant perfused vessel density (69±72 and 65±56 vessels/mm² in "Decrease" and "Increase I" groups) (**Figure 7B**).

Correlation between PET and histology

While no correlation between hypoxic fraction and SUV was found for the AT1-subline, a mod-

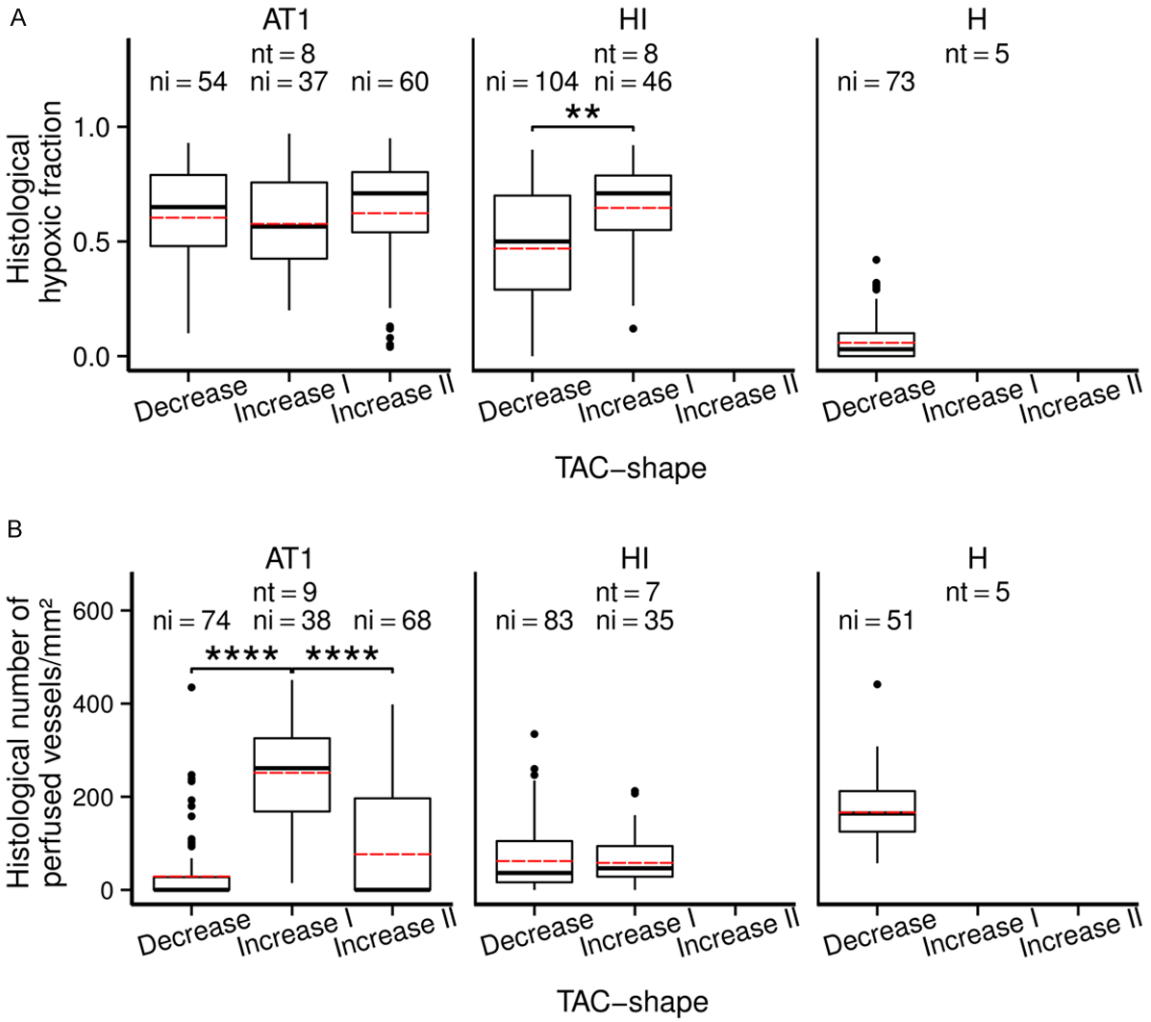

Figure 7. Histological parameters separated according to the respective tumor TAC-shape. (A) Hypoxic fraction and (B) number of perfused vessels (Solid line: median, dashed line: mean, box: 25/75 percentile, upper whisker: extends from the upper hinge to the highest value within 1.5×IQR, lower whisker: extends from the lower hinge to the lowest value within 1.5×IQR, dots: outliers, **P<0.01, ****P<0.0001 and nt and ni are the number of tumors and images analyzed, respectively).

erate correlation was seen for the HI- (r=0.64) and H-sublines (r=0.67). Likewise, pimonidazole mean intensity and SUV were not correlated in AT1-tumors but moderately correlated in HI- (r=0.64) and stronger in H-tumors (0.76). This similar result is partly explained by the strong correlation found between pimonidazole intensity and hypoxic fraction (**Figure 8**) for AT1- and H-sublines (r=0.78 and 0.89) and a moderate correlation for HI (r=0.59). Finally, hypoxic fraction and kinetic parameters k_3 and K_1 were either weakly or not at all correlated. Nonetheless, the mean values related to hypoxia for static PET and histology (SUV and HF), showed the same tendency, when normalized to the mean values of AT1 (**Table 1**), with the H-subline being least and the AT1-subline being most hypoxic.

Discussion

In this study, we characterized the hypoxic status of the AT1-, HI- and H-sublines of the Dunning R3327 rat prostate adenocarcinoma which differ in volume doubling time (VDT), androgen sensitivity, and progression status, using static and dynamic FMISO-PET-CT measurements as well as immunohistochemical stainings. Prostate tumors are assumed to exhibit significant levels of hypoxia [20-22] but only few clinical and preclinical *in vivo* studies with PET are available [23-27]. Therefore this

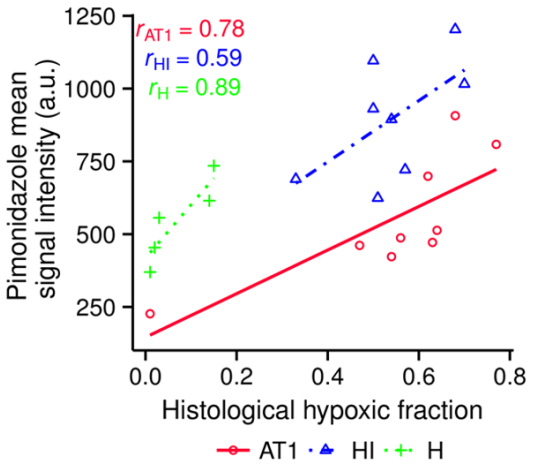

Figure 8. Correlation of mean signal intensity of pimonidazole and hypoxic fraction for each tumor subline.

study might be helpful to further validate the PET technique with prostatic tumor sublines.

PET-measurements analyzed by tumor sublines

In our study, AT1- and HI-sublines showed a significant FMISO-uptake for the large but not for the small tumors. This indicates that hypoxia is related to volume, which has been reported previously [41, 42]. We also found that the mean values of the SUV and HF for the large AT1-tumors were significantly higher than for the large H-tumors. While the H-subline can be then considered as well oxygenated, the AT1-subline is strongly hypoxic. This is also confirmed by the dynamic PET-analysis, which showed larger values of the hypoxia-related parameters k_3 and K_i for the AT1- in comparison to the H-subline. On the other hand, the HI-subline demonstrated a highly heterogeneous behavior with respect to the hypoxia-related parameters in the dynamic analysis.

Yeh *et al.*, measured the oxygen concentration of AT- and H-sublines using polarographic needles and in agreement with our results, they found that H-subline was significantly less hypoxic than the anaplastic tumor AT [43]. Zhao *et al.*, studied the hypoxic status of AT1- and H-sublines using the MRI-FREDOM technique (Fluorocarbon Relaxometry Using Echo Planar Imaging for Dynamic Oxygen Mapping) after injecting the reporter molecule Hexafluorobenzene into the tumor. As a result, the HF for the AT1- was larger than for the H-subline [44].

In another study, the same authors compared the hypoxic levels of the sublines HI and MAT-Lu [45], and the values of HF for HI were also lower than those they obtained for the AT1-subline in the AT1 and H study [44].

Although the HI-tumors showed a lower SUV than AT1-tumors, k_3 and K_i were higher and more dispersed. This finding might be explained by the fact that the fitting of the TAC was generally not as good for the HI- as compared to the AT1- and H-sublines. In accordance with this, we found significantly reduced k_3-values for the HI-tumors, when we repeated the fitting of the TAC and additionally constrained k_4 to zero (data not shown). This would not be expected, if FMISO is irreversibly bound to hypoxic cells [26], and suggests that the two-tissue compartment model, might have some limitations when applied to the HI-subline. In agreement to our findings, Busk *et al.*, concluded that a two-compartment model might be inappropriate in some tumor models [46].

Histological images analyzed by tumor sublines

For the AT1-subline, the HF and number of images without perfused vessels increased towards the center of the tumors, whereas this was not the case for the other two sublines. This suggests that hypoxia in the AT1-subline is related to a decreased perfusion although it has to be considered that the Hoechst 33342 dye was administered only 30 s before sacrificing the animal and thus impact of a limited diffusion time cannot be ruled-out. On the other hand, in the H-subline, non-perfused vessels were not observed at all and the size of vessels was the largest of all sublines, suggesting the presence of oxic conditions in this tumor.

Zhao *et al.* estimated the hypoxic fractions with pimonidazole and found 18% and 5% for the AT1- and H-sublines, respectively. These values, however, were significantly lower than those measured with the MRI-FREDOM technique (65% and 31% for pO_2<5 Torr), which suggests a dependence on the detection method. Using pimonidazole, we found HF of 62% for the AT1 and 7% for the H, which confirms that AT1 is the most hypoxic subline. In addition, Zhao *et al.* measured vascular densities for the AT1- and H-subline, however, they did not differentiate whether the vessels were perfused or not, and in another study with the HI-subline, they

Table 1. Mean values (±1SD) of the hypoxic parameters normalized to those of the AT1

Tumor subline	Number of animals	Hypoxic fraction	SUV (PET)	k_3 (1/min)	K_i (1/min)
AT1	8 (9 for SUV)	1.00±0.21	1.00±0.55	1.00±0.80	1.00±0.73
HI	10	0.87±0.23	0.84±0.71	5.49±4.69	3.73±2.88
H	8	0.11±0.11	0.47±0.22	0.05±0.06	0.08±0.09

only considered a qualitative comparison between total and perfused vessel density, which may explain the large differences to our study [44, 47]. The radial distribution of the HF for AT1-tumors showed that this subline develops a hypoxic core. This finding demonstrates spatial heterogeneity within a single tumor.

PET-measurements analyzed by TAC-shapes

According to Thorwarth *et al.* [48], TAC shapes provide important information on the perfusion and hypoxia level of the tumors. While the beginning of the curve is related to perfusion, the end of the curve describes the uptake, which in case of FMISO is related to hypoxia. In the dynamic PET-analysis, we found different TAC-shapes not only between but also within the sublines. Especially the AT1-subline showed 3 different TAC-shapes, suggesting 3 different levels of perfusion and hypoxia. This intra subline heterogeneity, however, is not a general finding in all tumors as shown by our results in the H-subline as well as by measurements of Sørensen *et al.*, who found different types of TAC-shapes only between two tumor types (C3H mammary carcinoma and squamous cell carcinoma SCCVII) [49].

Due to the heterogeneity observed within the AT1- and HI-sublines in the PET-analysis, we classified the tumors according to their TAC-shape and repeated the PET-analysis. As a result, we found for the AT1- and HI-sublines that SUV and K_i increase from TAC-shape type "Decrease", "Increase I" to "Increase II". This suggests that in "Increase II"-type AT1-tumors are most hypoxic.

With respect to the pharmacokinetic parameters, the global influx (K_i) seemed to be a more sensitive and robust measure for hypoxia. This is in accordance to Busk *et al.*, who reported for FAZA-PET measurements that K_i displayed less variability and correlated strongly with late time retention in 3 squamous cell carcinoma (SCC) tumor models [46].

Correlation between PET and histology

The measured differences between the sublines in our PET-study agree well with the results of published studies. However, in contrast to Dubois *et al.*, who described a strong correlation (r=0.9) between the hypoxic volume of FMISO-uptake and pimo-positive volume for rhabdomyosarcoma (R1) [50], we found no correlation between PET-SUV and kinetic parameters with the HF measured on the histological level (pimonidazole staining) for AT1-subline and only a moderate correlation for the HI- and H-sublines. This can also be seen in **Figure 7A** where HF and TAC-shape reveal no clear dependence for AT1-tumors, while the HI-tumors showed an increased HF when moving from the "Decrease" to the "Increase I" TAC-shape. The lack of correlation for AT1 might be explained by intertumoral heterogeneity, as large differences can be seen in the perfused vessel densities in this subline (**Figure 7B**). The HI-tumors on the other hand, demonstrated a rather constant perfused vessel density. While FMISO-uptake requires hypoxia as well as perfused vessels, that can deliver the tracer into the tumor, no-uptake can be a result of either oxic conditions or a low perfused vessel density. Perfusion differences may thus significantly impact PET and histology measurements. An additional limitation of our study is the lack of a spatial correlation between PET and histology, which also differ in resolution and sensitivity.

More homogeneously distributed tumor volumes and longer PET measuring times which may result in higher SUVs and thus in an improved signal to noise ratio, are possible improvements for future studies. However, no major changes in the TAC are expected for longer measuring times, as showed by O'Donogue *et al.* in AT-tumors [25]. Despite the limitations mentioned above, PET and histology independently showed the different hypoxic status of the three sublines. Furthermore, a comparison between hypoxic fraction and pimonidazole mean signal intensities for each subline, which

are both based on histological analysis, led to moderate and strong correlations (**Figure 8**).

Conclusions

Static PET and histological techniques were able to discriminate different hypoxic conditions of the AT1-, HI- and H-sublines of the Dunning R3327 rat prostate adenocarcinoma. In accordance with published data, the AT1 was the most hypoxic subline and exhibited the highest HF and the least perfusion in the center of the tumor. In contrast, the H-subline proved to be the most homogeneous one and provided oxic conditions. The HI-subline presented intermediate conditions and showed the largest inter-tumoral heterogeneity in the PET hypoxia-related parameters. Additional information on heterogeneity within each subline was obtained from dynamic PET-analysis by classifying the tumors according to their TAC-shape. The results demonstrate impact and limitations of static and dynamic PET-CT measurements to assess hypoxia non-invasively and *in vivo*.

Acknowledgements

The authors would like to thank Karin Leotta for her excellent technical support. This work was partially funded by CONICYT, Becas Chile.

Disclosure of conflict of interest

None.

Address correspondence to: Christian P Karger, Department of Medical Physics in Radiation Oncology (E040), German Cancer Research Center, Heidelberg, Germany. Tel: +49-6221-56-38965; Fax: +49-6221-56-4631; E-mail: c.karger@dkfz.de

References

[1] Gray LH, Conger AD, Ebert M, Hornsey S and Scott OC. The concentration of oxygen dissolved in tissues at the time of irradiation as a factor in radiotherapy. Br J Radiol 1953; 26: 638-648.

[2] Hockel M and Vaupel P. Tumor hypoxia: definitions and current clinical, biologic, and molecular aspects. J Natl Cancer Inst 2001; 93: 266-276.

[3] Walsh JC, Lebedev A, Aten E, Madsen K, Marciano L and Kolb HC. The clinical importance of assessing tumor hypoxia: relationship of tumor hypoxia to prognosis and therapeutic opportunities. Antioxid Redox Signal 2014; 21: 1516-1554.

[4] Nordsmark M, Overgaard M and Overgaard J. Pretreatment oxygenation predicts radiation response in advanced squamous cell carcinoma of the head and neck. Radiother Oncol 1996; 41: 31-39.

[5] Nordsmark M, Bentzen SM, Rudat V, Brizel D, Lartigau E, Stadler P, Becker A, Adam M, Molls M, Dunst J, Terris DJ and Overgaard J. Prognostic value of tumor oxygenation in 397 head and neck tumors after primary radiation therapy. An international multi-center study. Radiother Oncol 2005; 77: 18-24.

[6] Vaupel P, Hockel M and Mayer A. Detection and characterization of tumor hypoxia using pO2 histography. Antioxid Redox Signal 2007; 9: 1221-1235.

[7] Nozue M, Lee I, Yuan F, Teicher BA, Brizel DM, Dewhirst MW, Milross CG, Milas L, Song CW, Thomas CD, Guichard M, Evans SM, Koch CJ, Lord EM, Jain RK and Suit HD. Interlaboratory variation in oxygen tension measurement by Eppendorf "Histograph" and comparison with hypoxic marker. J Surg Oncol 1997; 66: 30-38.

[8] Willmann JK, van Bruggen N, Dinkelborg LM and Gambhir SS. Molecular imaging in drug development. Nat Rev Drug Discov 2008; 7: 591-607.

[9] Lopci E, Grassi I, Chiti A, Nanni C, Cicoria G, Toschi L, Fonti C, Lodi F, Mattioli S and Fanti S. PET radiopharmaceuticals for imaging of tumor hypoxia: a review of the evidence. Am J Nucl Med Mol Imaging 2014; 4: 365-384.

[10] Bentzen L, Keiding S, Horsman MR, Gronroos T, Hansen SB and Overgaard J. Assessment of hypoxia in experimental mice tumours by [18F] fluoromisonidazole PET and pO2 electrode measurements. Influence of tumour volume and carbogen breathing. Acta Oncol 2002; 41: 304-312.

[11] Rasey JS, Casciari JJ, Hofstrand PD, Muzi M, Graham MM and Chin LK. Determining hypoxic fraction in a rat glioma by uptake of radiolabeled fluoromisonidazole. Radiat Res 2000; 153: 84-92.

[12] Huang T, Civelek AC, Zheng H, Ng CK, Duan X, Li J, Postel GC, Shen B and Li XF. (18) F-misonidazole PET imaging of hypoxia in micrometastases and macroscopic xenografts of human non-small cell lung cancer: a correlation with autoradiography and histological findings. Am J Nucl Med Mol Imaging 2013; 3: 142-153.

[13] Okamoto S, Shiga T, Yasuda K, Ito YM, Magota K, Kasai K, Kuge Y, Shirato H and Tamaki N. High reproducibility of tumor hypoxia evaluated by 18F-fluoromisonidazole PET for head and neck cancer. J Nucl Med 2013; 54: 201-207.

[14] Sato J, Kitagawa Y, Yamazaki Y, Hata H, Okamoto S, Shiga T, Shindoh M, Kuge Y and Ta-

maki N. 18F-fluoromisonidazole PET uptake is correlated with hypoxia-inducible factor-1alpha expression in oral squamous cell carcinoma. J Nucl Med 2013; 54: 1060-1065.
[15] Cher LM, Murone C, Lawrentschuk N, Ramdave S, Papenfuss A, Hannah A, O'Keefe GJ, Sachinidis JI, Berlangieri SU, Fabinyi G and Scott AM. Correlation of hypoxic cell fraction and angiogenesis with glucose metabolic rate in gliomas using 18F-fluoromisonidazole, 18F-FDG PET, and immunohistochemical studies. J Nucl Med 2006; 47: 410-418.
[16] Nunn A, Linder K and Strauss HW. Nitroimidazoles and imaging hypoxia. Eur J Nucl Med 1995; 22: 265-280.
[17] Casciari JJ, Graham MM and Rasey JS. A modeling approach for quantifying tumor hypoxia with [F-18] fluoromisonidazole PET time-activity data. Med Phys 1995; 22: 1127-1139.
[18] Li F, Joergensen JT, Hansen AE and Kjaer A. Kinetic modeling in PET imaging of hypoxia. Am J Nucl Med Mol Imaging 2014; 4: 490-506.
[19] Kelada OJ and Carlson DJ. Molecular imaging of tumor hypoxia with positron emission tomography. Radiat Res 2014; 181: 335-349.
[20] Movsas B, Chapman JD, Hanlon AL, Horwitz EM, Pinover WH, Greenberg RE, Stobbe C and Hanks GE. Hypoxia in human prostate carcinoma: an Eppendorf PO2 study. Am J Clin Oncol 2001; 24: 458-461.
[21] Milosevic M, Warde P, Menard C, Chung P, Toi A, Ishkanian A, McLean M, Pintilie M, Sykes J, Gospodarowicz M, Catton C, Hill RP and Bristow R. Tumor hypoxia predicts biochemical failure following radiotherapy for clinically localized prostate cancer. Clin Cancer Res 2012; 18: 2108-2114.
[22] Taiakina D, Dal Pra A and Bristow RG. Intratumoral hypoxia as the genesis of genetic instability and clinical prognosis in prostate cancer. Tumor microenvironment and cellular stress: signaling, metabolism, imaging, and therapeutic targets. Adv Exp Med Biol 2014; 772: 189-204.
[23] Rasey JS, Koh WJ, Evans ML, Peterson LM, Lewellen TK, Graham MM and Krohn KA. Quantifying regional hypoxia in human tumors with positron emission tomography of [18F] fluoromisonidazole: a pretherapy study of 37 patients. Int J Radiat Oncol Biol Phys 1996; 36: 417-428.
[24] Garcia-Parra R, Wood D, Shah RB, Siddiqui J, Hussain H, Park H, Desmond T, Meyer C and Piert M. Investigation on tumor hypoxia in resectable primary prostate cancer as demonstrated by 18F-FAZA PET/CT utilizing multimodality fusion techniques. Eur J Nucl Med Mol Imaging 2011; 38: 1816-1823.
[25] O'Donoghue JA, Zanzonico P, Pugachev A, Wen B, Smith-Jones P, Cai S, Burnazi E, Finn RD, Burgman P, Ruan S, Lewis JS, Welch MJ, Ling CC and Humm JL. Assessment of regional tumor hypoxia using 18F-fluoromisonidazole and 64Cu (II)-diacetyl-bis (N4-methylthiosemicarbazone) positron emission tomography: Comparative study featuring microPET imaging, Po2 probe measurement, autoradiography, and fluorescent microscopy in the R3327-AT and FaDu rat tumor models. Int J Radiat Oncol Biol Phys 2005; 61: 1493-1502.
[26] Bartlett RM, Beattie BJ, Naryanan M, Georgi JC, Chen Q, Carlin SD, Roble G, Zanzonico PB, Gonen M, O'Donoghue J, Fischer A and Humm JL. Image-guided PO2 probe measurements correlated with parametric images derived from 18F-fluoromisonidazole small-animal PET data in rats. J Nucl Med 2012; 53: 1608-1615.
[27] Cho H, Ackerstaff E, Carlin S, Lupu ME, Wang Y, Rizwan A, O'Donoghue J, Ling CC, Humm JL, Zanzonico PB and Koutcher JA. Noninvasive multimodality imaging of the tumor microenvironment: registered dynamic magnetic resonance imaging and positron emission tomography studies of a preclinical tumor model of tumor hypoxia. Neoplasia 2009; 11: 247-259.
[28] Isaacs JT, Heston WD, Weissman RM and Coffey DS. Animal models of the hormone-sensitive and -insensitive prostatic adenocarcinomas, Dunning R-3327-H, R-3327-HI, and R-3327-AT. Cancer Res 1978; 38: 4353-4359.
[29] Tennant TR, Kim H, Sokoloff M and Rinker-Schaeffer CW. The Dunning model. Prostate 2000; 43: 295-302.
[30] Isaacs JT, Isaacs WB, Feitz WF and Scheres J. Establishment and characterization of seven Dunning rat prostatic cancer cell lines and their use in developing methods for predicting metastatic abilities of prostatic cancers. Prostate 1986; 9: 261-281.
[31] Glowa C, Peschke P, Karger CP, Hahn EW, Huber PE, Debus J and Ehemann V. Flow cytometric characterization of tumor subpopulations in three sublines of the Dunning R3327 rat prostate tumor model. Prostate 2013; 73: 1710-1720.
[32] Cheng C, Alt V, Dimitrakopoulou-Strauss A, Pan L, Thormann U, Schnettler R, Weber K and Strauss LG. Evaluation of new bone formation in normal and osteoporotic rats with a 3-mm femur defect: functional assessment with dynamic PET-CT (dPET-CT) using 2-deoxy-2-[(18) F] fluoro-D-glucose ((18)F-FDG) and (18) F-fluoride. Mol Imaging Biol 2013; 15: 336-344.
[33] Watabe H, Ikoma Y, Kimura Y, Naganawa M and Shidahara M. PET kinetic analysis--compartmental model. Ann Nucl Med 2006; 20: 583-588.
[34] Mikolajczyk K, Szabatin M, Rudnicki P, Grodzki M and Burger C. A JAVA environment for medical image data analysis: initial application for

brain PET quantitation. Med Inform (Lond) 1998; 23: 207-214.
[35] Burger C and Buck A. Requirements and implementation of a flexible kinetic modeling tool. J Nucl Med 1997; 38: 1818-1823.
[36] Pan L, Cheng C, Dimitrakopoulou-Strauss A, Haberkorn U and Strauss L. Machine learning based kinetic modeling: A robust and reproducible solution for PET data analysis. J Nucl Med Meeting Abstracts 2009; 50: 1427.
[37] Ohtake T, Kosaka N, Watanabe T, Yokoyama I, Moritan T, Masuo M, Iizuka M, Kozeni K, Momose T, Oku S and et al. Noninvasive method to obtain input function for measuring tissue glucose utilization of thoracic and abdominal organs. J Nucl Med 1991; 32: 1432-1438.
[38] Wang W, Georgi JC, Nehmeh SA, Narayanan M, Paulus T, Bal M, O'Donoghue J, Zanzonico PB, Schmidtlein CR, Lee NY and Humm JL. Evaluation of a compartmental model for estimating tumor hypoxia via FMISO dynamic PET imaging. Phys Med Biol 2009; 54: 3083-3099.
[39] Schneider CA, Rasband WS and Eliceiri KW. NIH Image to ImageJ: 25 years of image analysis. Nat Methods 2012; 9: 671-675.
[40] R Core Team. R: A language and environment for statistical computing. Vienna, Austria: R Foundation for Statistical Computing; 2013.
[41] Zhao D, Constantinescu A, Hahn EW and Mason RP. Tumor oxygen dynamics with respect to growth and respiratory challenge: investigation of the Dunning prostate R3327-HI tumor. Radiat Res 2001; 156: 510-520.
[42] Mason RP, Constantinescu A, Hunjan S, Le D, Hahn EW, Antich PP, Blum C and Peschke P. Regional tumor oxygenation and measurement of dynamic changes. Radiat Res 1999; 152: 239-249.
[43] Yeh KA, Biade S, Lanciano RM, Brown DQ, Fenning MC, Babb JS, Hanks GE and Chapman DC. Polarographic needle electrode measurements of oxygen in rat prostate carcinomas: accuracy and reproducibility. Int J Radiat Oncol Biol Phys 1995; 33: 111-118.
[44] Zhao D, Ran S, Constantinescu A, Hahn EW and Mason RP. Tumor oxygen dynamics: correlation of in vivo MRI with histological findings. Neoplasia 2003; 5: 308-318.
[45] Zhao D, Constantinescu A, Hahn EW and Mason RP. Differential oxygen dynamics in two diverse Dunning prostate R3327 rat tumor sublines (MAT-Lu and HI) with respect to growth and respiratory challenge. Int J Radiat Oncol Biol Phys 2002; 53: 744-756.
[46] Busk M, Munk OL, Jakobsen S, Wang T, Skals M, Steiniche T, Horsman MR and Overgaard J. Assessing hypoxia in animal tumor models based on pharmocokinetic analysis of dynamic FAZA PET. Acta Oncol 2010; 49: 922-933.
[47] Zhao D, Constantinescu A, Chang CH, Hahn EW and Mason RP. Correlation of tumor oxygen dynamics with radiation response of the dunning prostate R3327-HI tumor. Radiat Res 2003; 159: 621-631.
[48] Thorwarth D, Eschmann SM, Scheiderbauer J, Paulsen F and Alber M. Kinetic analysis of dynamic 18F-fluoromisonidazole PET correlates with radiation treatment outcome in head-and-neck cancer. BMC Cancer 2005; 5: 152.
[49] Sorensen M, Horsman MR, Cumming P, Munk OL and Keiding S. Effect of intratumoral heterogeneity in oxygenation status on FMISO PET, autoradiography, and electrode Po2 measurements in murine tumors. Int J Radiat Oncol Biol Phys 2005; 62: 854-861.
[50] Dubois L, Landuyt W, Haustermans K, Dupont P, Bormans G, Vermaelen P, Flamen P, Verbeken E and Mortelmans L. Evaluation of hypoxia in an experimental rat tumour model by [(18)F] fluoromisonidazole PET and immunohistochemistry. Br J Cancer 2004; 91: 1947-1954.